Asociación Argentina
de Mecánica Computacional

Mecánica Computacional Vol XXXI, págs. 2469-2484 (artículo completo)
Alberto Cardona, Paul H. Kohan, Ricardo D. Quinteros, Mario A. Storti (Eds.)
Salta, Argentina, 13-16 Noviembre 2012

THE SHEAR DEFORMATION EFFECT ON THE NONLINEAR DYNAMIC OF A SIMPLE ROTOR BLADE

Sebastián P. Machado[a,b] **and Cesar M. Saravia**[a,b]

[a]*Grupo Análisis de Sistemas Mecánicos, Centro de Investigaciones de Mecánica Teórica y Aplicada, Universidad Tecnológica Nacional FRBB. 11 de Abril 461, B8000LMI, Bahía Blanca. Argentina*
smachado@frbb.utn.edu.ar, msaravia@frbb.utn.edu.ar

[b]*Consejo Nacional de Investigaciones Científicas y Tecnológicas. Argentina*

Keywords: Composite material, thin-walled rotating beam, non-linear dynamic.

Abstract. The nonlinear planar response of a cantilever rotating slender beam to a principal parametric resonance of its first bending mode is analyzed considering the effect of shear deformation. The equation of motion is obtained in the form of an integro-partial differential equation, taking into account mid-plane stretching, a rotation speed and modal damping. A composite linear elastic material is considered and the cross-section properties are assumed to be constant given the assumption of small strains. The beam is subjected to a harmonic transverse load in the presence of internal resonance. The internal resonance can be activated for a range of the beam rotating speed, where the second natural frequency is approximately three times the first natural frequency. The method of multiple scales method is used to derive four-first ordinary differential equations that govern the evolution of the amplitude and phase of the response. These equations are used to determine the steady state responses and their stability. Nonlinear normal modes are obtained for the two models, considering and neglecting the effect of shear deformation. The results of the analysis show that the equilibrium solutions are influenced by the transverse shear effect. When this effect is ignored the amplitude of vibration is reduced significantly, thus altering the dynamic response of the beam. This alteration can lead to an incorrect stability prediction of the periodic solutions.

1 INTRODUCTION

Vibrations of rotating blades or beams have been a subject of constant research interest since they are applied in the design of helicopter blades, turbopropeller blades, wind-turbine blades and robotic arms. The most simplified representation of a rotating beam is a one-dimensional Euler-Bernoulli model. A uniform rotating beam of doubly symmetric cross-section is a special case (no torsional motion: i.e., out-of-plane (flapping) vibration and in-plane (lead-lag) vibration are uncoupled). Owing to the stiffening effect of the centrifugal tension, one can expect the natural frequencies to increase with an increase in the speed of rotation. In several publications a cantilever beam under rotating speed has been considered and approximate methods such as Rayleigh-Ritz, Galerkin, finite element methods, etc., has been used to derive natural frequencies (Schilhansl, 1958; Wang et al. 1976; Leissa, 1981; Hodges and Rutkowski, 1981). However, the nonlinear dynamic analysis of rotating beam is rather rare in the literature (Pesheck et al. 2002a, b; Apiwattanalunggarn et al. 2003; Turhan and Bulut, 2009). Systematic procedures have been developed to obtain reduced-order models (ROMs) via nonlinear normal modes (NNMs) that are based on invariant manifolds in the state space of nonlinear systems (Shaw and Pierre 1993, 1994; Shaw et al., 1999). These procedures initially used asymptotic series to approximate the geometry of the invariant manifold and have been used to study the nonlinear rotating Euler–Bernoulli beam (Pesheck et al., 2002a). Pesheck et al. (2002b) employed a numerically-based Galerkin approach to obtain the geometry of the NNM invariant manifolds out to large amplitudes. These procedures can be applied to more general nonlinearities over wider amplitude ranges, and have been applied to study the vibrations of a rotating Euler–Bernoulli beam (Pesheck et al., 2001). Apiwattanalunggarn et al. (2003) presented a nonlinear one-dimensional finite-element model representing the axial and transverse motions of a cantilevered rotating beam, which is reduced to a single nonlinear normal mode using invariant manifold techniques. They used their approach to study the dynamic characteristics of the finite element model over a wide range of vibration amplitudes. As it can be noted, the interest of most of works about nonlinear dynamic of rotating beams are focus on the reduced-order model as the invariant manifold solution. Turhan and Bulut (2009) investigated the in plane nonlinear vibrations of a rotating beam via single- and two-degree-of-freedom models obtained through Galerkin discretization. They performed a perturbation analyses on single- and two-degree-of-freedom models to obtain amplitude dependent natural frequencies and frequency responses. In the last four references, the computational cost associated with generating the manifold solution and the efficiency of the resultant model was mainly analyzed.

On the other hand, the effect of shear flexibility in the case of composite materials is a phenomenon very important and crucial in some beam models. For example, it has been demonstrated the significance of this effect in linear and nonlinear static analysis (Sapkás and Kollár, 2002; Machado and Cortínez, 2005a,b; Sapountzakis and Mokos, 2008; Machado, 2010) and in linear dynamic cases (Machado et al., 2007; Machado and Cortínez, 2009). The objective of this paper is to analyze the influence of the shear deformation effect on the nonlinear dynamic response of a composite rotating beam. In particular, the case of internal resonance of a cantilever rotating beam subjected to a harmonic transverse load is explored. The modal interaction represents an interesting nonlinear dynamical problem to determine the influence of shear deformation on the numerical results.

Therefore the nonlinear planar vibration of a rotating cantilever beam with harmonic transverse load in the presence of internal resonance is analyzed. The model is based on one-dimensional formulation where the geometric cubic nonlinear terms are included in the equation of motion due to midline stretching of the beam. The linear frequencies of the

system are dependent on the rotation speed and this effect is used to activate the internal resonance. For a particular rotation speed the second natural frequency is approximately three times the first natural frequency and hence the first and second modes may interact due to a three-one internal resonance. Principal parametric resonance of first mode considering internal resonance is analyzed here. Principal parametric resonance of second mode in presence of 3:1 internal resonance is not considered here due to lack of space and is studied in another paper. For a comprehensive review of nonlinear modal interactions, we refer the reader to Nayfeh and Mook (1979), Nayfeh and Balachandran (1989), and Nayfeh (1996).

The method of multiple scales (MMS) is used to attack directly the governing nonlinear partial differential equation of motion of the beam and reduced the problem to sets of first-order nonlinear modulation equations in terms of the complex modes of the beam. These modulation equations are numerically analyzed for stability and bifurcations of trivial and nontrivial solutions. Bifurcation diagrams representing system responses with variation of parameters like amplitude and frequency of the lateral excitation load, frequency detuning of internal resonances and damping are computed with the help of a continuation algorithm (Nayfeh and Balachandran, 1995). The trivial state stability plots are presented. The effect of shear deformation is illustrated on the frequency response curves. The analysis is supplemented by considering the variation of the beam lengths, rotation speed, load amplitude, modal damping and internal resonance parameter.

2 NON-LINEAR EQUATIONS OF MOTION

We consider the dynamic response of a rotating box beam subjected to harmonic transverse loads (see Figure 1). The origin of the beam coordinate system (x, y, z) is located at the blade root at an offset R_0 from the rotation axis fixed in space. R_0 denotes the radius of the hub (considered to be rigid) in which the blade or beam is mounted and which rotates about its polar axis through the origin *0*. We assume that the motion is planar and the laminate stacking sequence is assumed to be symmetric and balanced (Barbero, 1999). A doubly symmetric cross-section box-beam is used and so out-of-plane (flapping) and in-plane (lead-lag) vibration are uncoupled. Considering rotary inertia and the transverse shear, the non-linear equations of motion of a rotating beam yields (Machado et al. 2007; Librescu, 2006):

$$\rho A\, \ddot{u} - EA\left(u' + \frac{1}{2} v'^2 \right)' - \rho A\left(R_0 + x + u \right)\Omega^2 = 0\,, \tag{1}$$

$$\rho A\, \ddot{v} - GS_y \left(v' - \theta_z \right)' - \left(N\, v' \right)' = F\cos(\varpi t)\,, \tag{2}$$

$$\rho I_Z\, \ddot{\theta}_z - EI_Z \theta_z'' - GS_y \left(v' - \theta_z \right) = 0\,, \tag{3}$$

where Ω is the beam rotation speed, ρA is the mass per unit length. EA, EI_z and GS_y are the axial, flexural and shear rigidity, ϖ is the excitation frequency, F describes the applied transverse harmonic load and N is the axial beam force. The axial and transverse displacements are denoted as u and v, respectively; while θ_z is the angle of rotation due to bending. Overdots indicate differentiation with respect to time and primes with respect to the axial co-ordinate.

If the inertial effects along the longitudinal direction are neglected and considering the radius of the hub R_0 = 0, by the direct integration the Eq. (1) in conjunction with the boundary condition of zero axial load at the free and then substituting the axial beam force expression

and making some arrangements on Eq. (2), the motion equations are:

$$\rho A\,\ddot{v} - GS_y\left(v'' - \theta_z'\right) + \rho A\, x\,\Omega^2 v' - \rho A\,\Omega^2\left(\frac{L^2}{6} - \frac{x^2}{2}\right)v'' - \frac{EA}{2L}v''\int_0^L v'^2 dx = F\cos(\varpi t), \quad (4)$$

$$\rho I_Z\ \ddot{\theta}_z - EI_Z\theta_z'' - GS_y\left(v' - \theta_z\right) = 0, \quad (5)$$

To eliminate the spatial dependence we introduce an approximation in Eq. (4) considering the average value of the axial and centrifugal force along the beam. Finally, introducing a nondimensional quantity for $x^* = x/L$ and dropping the asterisk the expressions can be conveniently rewritten as

$$\ddot{v} + \alpha_1 v'' + \alpha_2\theta_z' + \lambda v' - \chi v'' - \gamma v''\int_0^1 v'^2 \mathrm{dx} = f\cos(\varpi t), \quad (6)$$

$$\ddot{\theta}_z + \alpha_3\theta_z'' - \alpha_4 v' + \alpha_5\theta_z = 0. \quad (7)$$

On the other hand, the cantilever boundary conditions demand that

$$\begin{aligned} &v = 0 \quad \text{and} \quad \theta_z = 0 \quad \text{at } x = 0, \\ &v'' = 0 \ \text{ and } \ \theta_z'' = 0 \quad \text{at } x = 1, \end{aligned} \quad (8)$$

where

$$\begin{aligned} &\alpha_1 = -\frac{GS_y}{\rho A\,L^2},\ \ \alpha_2 = \frac{GS_y}{\rho A\,L},\ \ \alpha_3 = -\frac{EI_z}{\rho I_z\,L^2},\ \ \alpha_4 = \frac{GS_y}{\rho I_z L},\ \ \alpha_5 = \frac{GS_y}{\rho I_z}, \\ &\chi = \frac{\Omega^2}{6},\ \ \gamma = \frac{EA}{2\rho A L^4},\ \ \lambda = \frac{\Omega^2}{2},\ \ \ f = \frac{F}{\rho A}. \end{aligned} \quad (9)$$

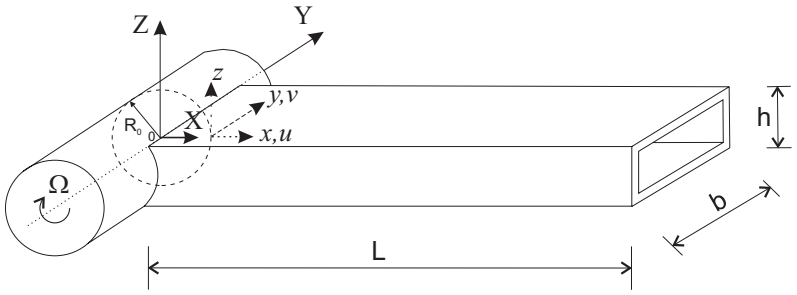

Figure 1. A schematic description of the rotating box beam.

3 METHOD OF ANALISIS

The present system of rotating cantilever beam is analyzed in the form of a first-order uniform expansion through the MMS applied directly to the partial differential Eqs. (6-7) and the associated boundary conditions Eq. (8). The direct perturbation technique has been used considering its advantage over the discretization perturbation technique (Nayfeh el al. 1992; Nayfeh, 1996). Though the direct perturbation method and the discretization-perturbation method, both for linear and nonlinear systems, yield identical results for infinite modes, the

former gives better results for finite mode truncation if a higher order perturbation scheme were used. In such a case, employing the direct perturbation method would be more straightforward, even though the algebra might be more involved.

We seek an approximate solution to this weakly nonlinear distributed parameter system in the form of a first-order uniform expansion and introduce the time scale $T_n = \varepsilon^n t$, $n = 0,1,2,...$ The time derivatives are

$$\frac{d}{dt} = D_0 + \varepsilon D_1 + ..., \quad \frac{d^2}{dt^2} = D_0^2 + 2\varepsilon D_0 D_1 + ..., D_n = \frac{\partial}{\partial T_n}, \quad n = 0,1,2,.... \tag{10}$$

A small parameter ε is introduced by ordering the linear damping and load amplitude as $\mu = \varepsilon\tilde{\mu}, f = \varepsilon\tilde{f}$. Moreover, the displacement $v(x,t)$ and the measure of the rotation $\theta_z(x,t)$ are expanded as:

$$v(x,t) = v_1(T_0, T_1, x) + \varepsilon\ v_2(T_0, T_1, x) + ... \tag{11}$$

$$\theta_z(x,t) = \theta_1(T_0, T_1, x) + \varepsilon\ \theta_2(T_0, T_1, x) + ... \tag{12}$$

Substituting Eqs. (10-12) into Eqs. (6-8) and equating coefficients of like powers of ε on both sides, we obtain

Order ε^0 :

$$\begin{cases} D_0^2 v_1 + \alpha_1 v_1'' + \alpha_2 \theta_1' - \chi v_1'' + \lambda v_1' = 0 \\ D_0^2 \theta_1 + \alpha_3 \theta_1'' - \alpha_4 v_1' + \alpha_5 \theta_1 = 0 \end{cases} \tag{13}$$

Order ε^1 :

$$\begin{cases} D_0^2 v_2 + \alpha_1 v_2^{iv} + \alpha_2 \theta_1' - \chi v_2'' + \lambda v_2' = -2D_0 D_1 v_1 - 2\mu_v D_0 v_1 - \gamma v_1'' \int_0^1 v_1'^2 \mathrm{dx} + f\cos(\varpi t) \\ D_0^2 \theta_2 + \alpha_3 \theta_2'' - \alpha_4 v_2' + \alpha_5 \theta_2 = -2D_0 D_1 \theta_1 - 2\mu_\theta D_0 \theta_1 \end{cases} \tag{14}$$

The solution to the first-order perturbation Eq. (13) can be expressed as

$$v_1(T_0, T_1, x) = \sum_{m=1}^{\infty} \vartheta_m(x) A_m(T_1) e^{i\omega_m T_0} + cc, \tag{15}$$

$$\theta_1(T_0, T_1, x) = \sum_{m=1}^{\infty} \phi_m(x) A_m(T_1) e^{i\omega_m T_0} + cc, \tag{16}$$

where $\phi_m(x)$ and $\vartheta_m(x)$ are the mode shapes, ω_m are the natural frequencies and *cc* stands for complex conjugate.

Substitution of Eqs. (15) and (16) into the set of Eq. (13) leads to the following expressions (omitting the notation of *x* dependence)

$$-\omega_m^2 \vartheta_m + \alpha_1 \vartheta_m'' + \alpha_2 \phi_m' - \chi \vartheta_m'' + \lambda \vartheta_m' = 0, \tag{17}$$

$$-\omega_m^2 \phi_m + \alpha_3 \phi_m'' - \alpha_4 \vartheta_m' + \alpha_5 \phi_m = 0. \tag{18}$$

Sorting out θ_m and v_m from Eqs. (17) and (18), respectively; the results are derived and replaced into the Eqs. (18) and (17) to decoupling both equations. Therefore, the following equations are obtained:

$$\begin{aligned}\beta_1\vartheta_m{}^{iv}+\beta_2\vartheta_m{}'''+\beta_3\vartheta_m{}''+\beta_4\vartheta_m{}'+\beta_5\vartheta_m=0\\ \beta_1\phi_m{}^{iv}+\beta_2\phi_m{}'''+\beta_3\phi_m{}''+\beta_4\phi_m{}'+\beta_5\phi_m=0\end{aligned}, \tag{19}$$

where

$$\begin{aligned}\beta_1=\alpha_3\left(\chi-\alpha_1\right),\ \ \beta_2=-\alpha_3\lambda,\ \ \beta_3=\alpha_5\chi-\alpha_2\alpha_4-\alpha_1\alpha_5+\omega^2\left(\alpha_1+\alpha_3-\chi\right),\\ \beta_4=\lambda\left(\omega^2-\alpha_5\right),\quad \beta_5=\omega^2\left(\alpha_5-\omega^2\right).\end{aligned} \tag{20}$$

Solving the set of Eq. (19) along with the specified cantilever boundary conditions, the mode shapes are obtained.

$$\begin{aligned}\vartheta_m(x)=\Big[&-e^{i(\lambda_1+x\lambda_4)}\left(h_2-h_3\right)\lambda_1^2+e^{i(\lambda_1+x\lambda_3)}\left(h_2-h_4\right)\lambda_1^2-e^{i(\lambda_1+x\lambda_2)}\left(h_3-h_4\right)\lambda_1^2+e^{i(\lambda_2+x\lambda_4)}\left(h_1-h_3\right)\lambda_2^2\\ &-e^{i(\lambda_2+x\lambda_3)}\left(h_1-h_4\right)\lambda_2^2+e^{i(\lambda_2+x\lambda_1)}\left(h_3-h_4\right)\lambda_2^2-e^{i(\lambda_3+x\lambda_4)}\left(h_1-h_2\right)\lambda_3^2+e^{i(\lambda_3+x\lambda_2)}\left(h_1-h_4\right)\lambda_3^2-\\ &-e^{i(\lambda_3+x\lambda_1)}\left(h_2-h_4\right)\lambda_3^2+e^{i(\lambda_4+x\lambda_3)}\left(h_1-h_2\right)\lambda_4^2-e^{i(\lambda_4+x\lambda_2)}\left(h_1-h_3\right)\lambda_4^2+e^{i(\lambda_4+x\lambda_1)}\left(h_2-h_3\right)\lambda_4^2\Big]\Big/\\ &\left[e^{i\lambda_2}\left(h_3-h_4\right)\lambda_2^2-e^{i\lambda_3}\left(h_2-h_4\right)\lambda_3^2+e^{i\lambda_4}\left(h_2-h_3\right)\lambda_4^2\right]\end{aligned} \tag{21}$$

$$\begin{aligned}\phi_m(x)=\Big[&e^{i(\lambda_1+x\lambda_3)}h_3\left(h_2-h_4\right)\lambda_1^2-e^{i(\lambda_1+x\lambda_2)}h_2\left(h_3-h_4\right)\lambda_1^2-e^{i(\lambda_1+x\lambda_4)}h_4\left(h_2-h_3\right)\lambda_1^2-e^{i(\lambda_2+x\lambda_3)}\\ &h_3\left(h_1-h_4\right)\lambda_2^2+e^{i(\lambda_2+x\lambda_1)}h_1\left(h_3-h_4\right)\lambda_3^2+e^{i(\lambda_2+x\lambda_4)}h_4\left(h_1-h_3\right)\lambda_2^2+e^{i(\lambda_3+x\lambda_2)}h_2\left(h_1-h_2\right)\lambda_3^2\\ &-e^{i(\lambda_3+x\lambda_1)}h_1\left(h_2-h_4\right)\lambda_3^2-e^{i(\lambda_3+x\lambda_4)}h_4\left(h_1-h_2\right)\lambda_3^2-e^{i(\lambda_4+x\lambda_2)}h_2\left(h_1-h_3\right)\lambda_4^2+e^{i(\lambda_4+x\lambda_1)}h_1\\ &\left(h_2-h_3\right)\lambda_4^2+e^{i(\lambda_4+x\lambda_3)}h_3\left(h_1-h_2\right)\lambda_4^2\Big]\Big/\Big[e^{i\lambda_2}\left(h_3-h_4\right)\lambda_2^2-e^{i\lambda_3}\left(h_2-h_4\right)\lambda_3^2+e^{i\lambda_4}\left(h_2-h_3\right)\lambda_4^2\Big]\end{aligned} \tag{22}$$

where λ_i are the eigenvalues which satisfy the relation

$$\beta_1\lambda_i^4-i\beta_2\lambda_i^3-\beta_3\lambda_i^2+i\beta_4\lambda_i+\beta_5=0\,,\qquad i=1,2,3,4 \tag{23}$$

and h_j are the coefficients that relate the solution of Eq. (19)

$$h_j=\frac{i}{\alpha_2\lambda_j}\left(-i\ \lambda\ \lambda_j+\alpha_1\lambda_j^2-\chi\lambda_j^2+\omega^2\right),\qquad j=1,2,3,4. \tag{24}$$

Finally, the characteristic equation is

$$\begin{aligned}&\left(h_2-h_3\right)\left(h_1-h_4\right)\left(e^{i(\lambda_2+\lambda_3)}\lambda_2^2\lambda_3^2+e^{i(\lambda_1+\lambda_4)}\lambda_1^2\lambda_4^2\right)+\left(h_1-h_3\right)\left(h_2-h_4\right)\left(-e^{i(\lambda_1+\lambda_3)}\lambda_1^2\lambda_3^2-e^{i(\lambda_2+\lambda_4)}\lambda_2^2\lambda_4^2\right)\\ &+\left(h_1-h_2\right)\left(h_3-h_4\right)\left(e^{i(\lambda_1+\lambda_2)}\lambda_1^2\lambda_2^2+e^{i(\lambda_3+\lambda_4)}\lambda_3^2\lambda_4^2\right)=0.\end{aligned} \tag{25}$$

The linear natural frequencies of the cantilever beam vary with the rotation speed for different modes for variation of parameters like flexural stiffness and beam mass. For specific

combinations of system parameters, the lower natural frequencies can be commensurable, leading to internal resonance in the system and nonlinear interaction between the associated modes. We analyze the specific case of two mode interaction corresponding to particular system parameters. A three-to-one internal resonance $\omega_2 \cong 3\omega_1$ is considered for a range of rotation beam speed. Since none of these first two modes is in internal resonance with any other mode of the beam, all other modes except the directly or indirectly excited first or second mode decay with time due to the presence of damping and the first two modes will contribute to the long term system response (Nayfeh, 1996). Hence we can replace Eqs. (15) and (16) by

$$v_1(T_0,T_1,x) = A_1(T_1)\vartheta_1(x)e^{i\omega_1 T_0} + A_2(T_1)\vartheta_2(x)e^{i\omega_2 T_0} + cc, \tag{26}$$

$$\theta_1(T_0,T_1,x) = A_1(T_1)\phi_1(x)e^{i\omega_1 T_0} + A_2(T_1)\phi_2(x)e^{i\omega_2 T_0} + cc, \tag{27}$$

where *cc* stands for the complex conjugate of the preceding terms and A_i are the unknown complex-valued functions. In order to investigate the system response under internal and external resonance conditions, two detuning parameters σ_i are introduced:

$$\omega_2 = 3\omega_1 + \varepsilon\ \sigma_1, \quad \varpi = \omega_1 + \varepsilon\ \sigma_2. \tag{28}$$

Substituting Eqs. (26-27) and (28) into the set of Eq. (14),

$$\begin{cases} D_0^2 v_2 + \alpha_1 v_2^{iv} + \alpha_2\theta_1' - \chi v_2'' + \lambda v_2' = \Gamma_1(T_1,x)e^{i\omega_1 T_0} + \Gamma_2(T_1,x)e^{i(3\omega_1 T_0+\sigma_1 T_1)} \\ \qquad\qquad + \dfrac{1}{2} f\ e^{i(\omega_1 T_0+\sigma_1 T_2)} + cc + NST, \\ D_0^2\theta_2 + \alpha_3\theta_2'' - \alpha_4 v_2' + \alpha_5\theta_2 = \Gamma_3(T_1,x)e^{i\omega_1 T_0} + \Gamma_4(T_1,x)e^{i(3\omega_1 T_0+\sigma_1 T_1)} + cc + NST, \end{cases} \tag{29}$$

where the terms Γ_m are defined in Appendix. *NST* stands for terms that do not produce secular or small divisor terms. As the homogeneous part of Eq. (29) with its associated boundary conditions has a nontrivial solution, the corresponding nonhomogeneous problem has a solution only if a solvability condition is satisfied (Nayfeh and Mook, 1979). This requires the right-hand side of Eq. (29) to be orthogonal to every solution of the adjoint homogeneous problem, which leads to the following complex variable modulation equations for the amplitude and phase

$$2i\left(A_1' + \mu_1 A_1\right) + 8A_1\left(\gamma_{11}A_1\bar{A}_1 + \gamma_{12}A_2\bar{A}_2\right) + 8\delta_1 A_2\bar{A}_1{}^2 e^{i\sigma_1 T_1} - \frac{1}{2} f_1 e^{i\sigma_2 T_1} = 0, \tag{30}$$

$$2i\left(A_2' + \mu_2 A_2\right) + 8A_2\left(\gamma_{21}A_1\bar{A}_1 + \gamma_{22}A_2\bar{A}_2\right) + 8\delta_2 A_1{}^3 e^{-i\sigma_1 T_1} = 0, \tag{31}$$

where prime denotes differentiation with respect to the slow time T_1 and μ_m, γ_m, δ_m and f_1 are defined in Appendix. Overbar indicates complex conjugate. The terms in the above equations involving the internal frequency detuning parameter σ_1 are the contributions of internal resonance in the system.

Introducing a Cartesian coordinates Eq. (32), the following amplitude and phase Eqs. (33-36) are finally obtained:

$$A_k = \frac{1}{2}\left[p_k(T_1) - iq_k(T_1)\right]e^{i\nu_k T_1} \qquad k = 1,2. \tag{32}$$

$$p_1' = -\mu_1 p_1 - \nu_1 q_1 + \gamma_{11} q_1 \left(p_1^{\,2} + q_1^{\,2} \right) + \gamma_{12} q_1 \left(p_2^{\,2} + q_2^{\,2} \right) - \delta_1 \left[2 p_1 q_1 p_2 - q_2 \left(p_1^{\,2} + q_1^{\,2} \right) \right], \tag{33}$$

$$q_1' = -\mu_1 q_1 + \nu_1 p_1 - \gamma_{11} p_1 \left(p_1^{\,2} + q_1^{\,2} \right) - \gamma_{12} p_1 \left(p_2^{\,2} + q_2^{\,2} \right) - \delta_1 \left[2 p_1 q_1 q_2 + p_2 \left(p_1^{\,2} - q_1^{\,2} \right) \right] + \frac{1}{2} f_1, \tag{34}$$

$$p_2' = -\mu_2 p_2 - \nu_2 q_2 + \gamma_{21} q_2 \left(p_1^{\,2} + q_1^{\,2} \right) + \gamma_{22} q_2 \left(p_2^{\,2} + q_2^{\,2} \right) + \delta_2 q_1 \left(3 p_1^{\,2} - q_1^{\,2} \right), \tag{35}$$

$$q_2' = -\mu_2 q_2 + \nu_2 p_2 - \gamma_{21} p_2 \left(p_1^{\,2} + q_1^{\,2} \right) - \gamma_{22} p_2 \left(p_2^{\,2} + q_2^{\,2} \right) + \delta_2 p_1 \left(3 q_1^{\,2} - p_1^{\,2} \right), \tag{36}$$

where

$$\nu_1 = \sigma_2, \qquad \nu_2 = 3\sigma_2 - \sigma_1 \tag{37}$$

and the prime indicates the derivative with respect to T_1.

4 EULER-BERNOULLI BEAM MODEL

The purpose of this section is to present the unshearable beam model used to compare the nonlinear dynamic results obtained with the present model. Neglecting rotary inertia and the transverse shear, the non-linear equations of motion of a rotating beam yields (Machado and Saravia, 2010):

$$\rho A\, \ddot{v} + EI\; v^{iv} - \left[\frac{EA}{2L} \int_0^L v'^2 \mathrm{dx} + \frac{\Omega^2 \rho A}{2} \left(\frac{L^2}{3} - x^2 \right) \right] v'' + \rho A \Omega^2 v' x = F \cos(\varpi t). \tag{38}$$

Introducing a nondimensional quantity for $x^* = x / L$, substituting this relationship in Eq. (38) with the corresponding boundary conditions, adding damping μ, and dropping the asterisk the expressions can be conveniently rewritten as:

$$\ddot{v} + \alpha v^{iv} + 2\mu\dot{v} - \chi v'' - \gamma v'' \int_0^1 v'^2 \mathrm{dx} + \lambda v' = f \cos(\varpi t), \quad BC \begin{cases} v = 0 \quad \text{and} \quad v' = 0 \quad \text{at } x = 0 \\ v'' = 0 \quad \text{and} \quad v''' = 0 \quad \text{at } x = 1 \end{cases}. \tag{39}$$

Following the same methodology of MMS, as described in the previous section 3, we arrive to the same modulation equations Eqs. (33-36). The main difference between both models (with and without shear deformation effect), is in the eigenvalues and modes used to obtain the coefficients that govern the modulation equations. In this case the unshearable mode shapes $\vartheta_m(x)$ of the rotating cantilever beam is:

$$\begin{aligned} \vartheta_m(x) = e^{x\beta_{4m}} + \Big\{ & e^{x\beta_{3m}} \left[-e^{\beta_{2m}} \beta_{2m}^2 (\beta_{1m} - \beta_{4m}) + e^{\beta_{1m}} \beta_{1m}^2 (\beta_{2m} - \beta_{4m}) + e^{\beta_{4m}} \beta_{4m}^2 (\beta_{1m} - \beta_{2m}) \right] \\ & + e^{x\beta_{2m}} \left[e^{\beta_{3m}} \beta_{3m}^2 (\beta_{1m} - \beta_{4m}) - e^{\beta_{1m}} \beta_{1m}^2 (\beta_{3m} - \beta_{4m}) - e^{\beta_{4m}} \beta_{4m}^2 (\beta_{1m} - \beta_{3m}) \right] \\ & + e^{x\beta_{1m}} \left[-e^{\beta_{3m}} \beta_{3m}^2 (\beta_{2m} - \beta_{4m}) + e^{\beta_{2m}} \beta_{2m}^2 (\beta_{3m} - \beta_{4m}) + e^{\beta_{4m}} \beta_{4m}^2 (\beta_{2m} - \beta_{3m}) \right] \Big\} \Big/ \Big[-e^{\beta_{2m}} \beta_{2m}^2 \\ & (\beta_{1m} - \beta_{3m}) + e^{\beta_{1m}} \beta_{1m}^2 (\beta_{2m} - \beta_{3m}) + e^{\beta_{3m}} \beta_{3m}^2 (\beta_{1m} - \beta_{2m}) \Big]. \end{aligned} \tag{40}$$

where β_{im} are the eigenvalues which satisfy the relation

$$\alpha \beta_{im}^4 - \chi \beta_{im}^2 + \lambda \beta_{im} - \omega_m^2 = 0, \qquad i = 1,2,3,4 \tag{41}$$

and the characteristic equation is:

$$
\begin{aligned}
&(\beta_{2n}-\beta_{3n})(\beta_{1m}-\beta_{4m})\left(e^{\beta_{2n}+\beta_{3n}}\beta_{2n}^2\beta_{3n}^2+e^{\beta_{1n}+\beta_{4n}}\beta_{1n}^2\beta_{4n}^2\right)\\
&+(\beta_{1n}-\beta_{3n})(\beta_{2m}-\beta_{4m})\left(-e^{\beta_{1n}+\beta_{3n}}\beta_{1n}^2\beta_{3n}^2-e^{\beta_{2n}+\beta_{4n}}\beta_{2n}^2\beta_{4n}^2\right)\\
&+(\beta_{1n}-\beta_{2n})(\beta_{3m}-\beta_{4m})\left(e^{\beta_{1n}+\beta_{2n}}\beta_{1n}^2\beta_{2n}^2+e^{\beta_{3n}+\beta_{4n}}\beta_{3n}^2\beta_{4n}^2\right)=0.
\end{aligned}
\tag{42}
$$

5 RESULTS AND DISCUSSION

For the analysis of the rotating beam subjected to principal parametric resonance of the first mode (i.e., $\varpi \cong \omega_1$) in presence of 3:1 internal resonance, system parameters are taken as mentioned earlier corresponding to the commensurable natural frequencies of the first and second mode of the system. The second natural frequency and three times the first natural frequency are plotted as functions of Ω in Figure 2. As it can be observed, the internal resonance is perfectly tuned when Ω is 529 rpm. The beam geometrical characteristics used are: L = 15 m, h = 0.3 m, b = 0.7 m, e = 0.05 m. The analyzed material is graphite-epoxy whose properties are E_1 = 144 GPa, E_2 = 9.65 GPa, G_{12} = 4.14 GPa, G_{13}=4.14 GPa, G_{23} = 3.45 GPa, ν_{12} = 0.3, ν_{13} = 0.3, ν_{23} = 0.5, for a sequence of lamination {*0/0/0/0*}.

The influence of shear deformation is analyzed for the natural frequencies in function of the rotation speed. When the shear effect is neglected (see Fig. 2b), ω_2 is larger in comparison with its inclusion (see Fig. 2a) and the internal resonance is tuned for a larger rotation speed of about 810 rpm. It can be noticed that in this case the first frequency ω_1 is very similar in both models due to the beam slenderness (h/L = 0.02). However, the second frequency obtained without shear effect disagrees with the present model in about 32%, for the non-rotating beam condition.

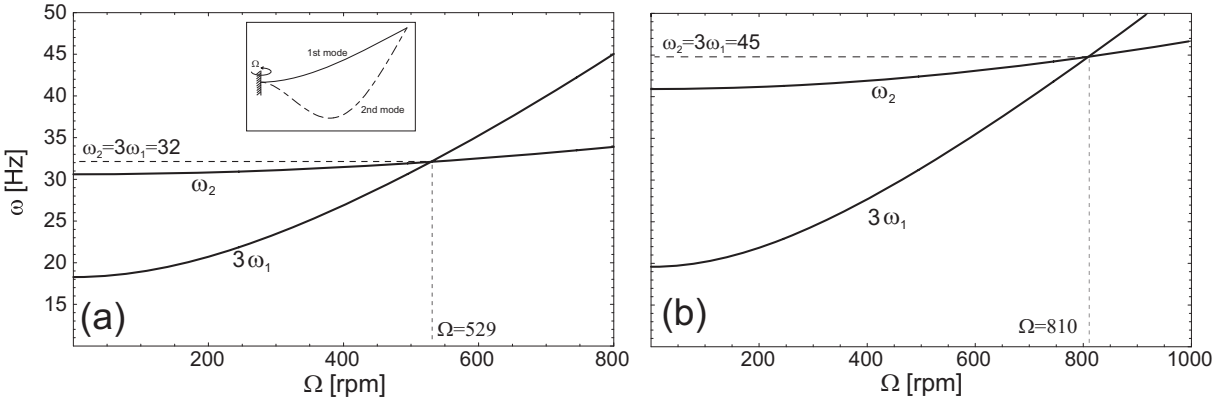

Figure 2. Variations of three times the first ω_1 and second ω_2 natural frequencies with the rotation speed Ω. (a) with and (b) without shear deformation effect.

The equilibrium solutions of Eqs. (33-36) correspond to periodic motions of the beam. Steady-state solutions are determined by zeroing $p_i' = q_i' = 0$ the right-hand members of the modulation Eqs. (33-36) and solving the non-linear system. Stability analysis is then performed by analyzing the eigenvalues of the Jacobian matrix of the non-linear equations calculated at the fixed points. The frequency-response curves are shown in Figure 3, for an internal and external resonance condition and considering two forcing amplitude values f = 0.05 and 0.025. The modal amplitude a_i curves are obtained in function of the external detuning parameter σ_2. In this case, modal damping d_i = 0.05 and internal detuning parameter σ_1= 0.04. The amplitudes a_1 and a_2 are obtained by means of the following expression:

$$a_i = \sqrt{p_i^{\,2} + q_i^{\,2}} \qquad i = 1,2. \tag{43}$$

The corresponding nonlinear interaction coefficients defined in Eqs. (30) and (31), are presented in Table 1. The coefficients correspond to a specific value of the rotating speed Ω = 326.82 rpm for which ω_1 = 10.67 Hz and ω_2 = 32 Hz in the case of the present model and ω_1 = 10.82 Hz and ω_2 = 42.3 Hz when shear effect in neglected.

Table 1. Coefficients of the modulation equations, Eqs. (30 and 31) for L= 15 m and Ω = 326.82 rpm.

Model	γ_{11}	γ_{12}	γ_{21}	γ_{22}	δ_1	δ_2
With shear	30.9	910.5	-112.1	-669.5	-146.7	6.4
Without shear	26.5	842.3	-87.5	-599.2	-136.5	4.5

The response curve corresponding to the first amplitude shows a noticeable hardening-spring type behavior for both forcing amplitude (Figure 3a and 3c). The amplitude of the indirectly excited second mode is smaller in comparison with the first mode (Figure 3b and 3d). In the Figures, solid (dotted) lines denote stable (unstable) equilibrium solutions and thin solid lines denote unstable foci.

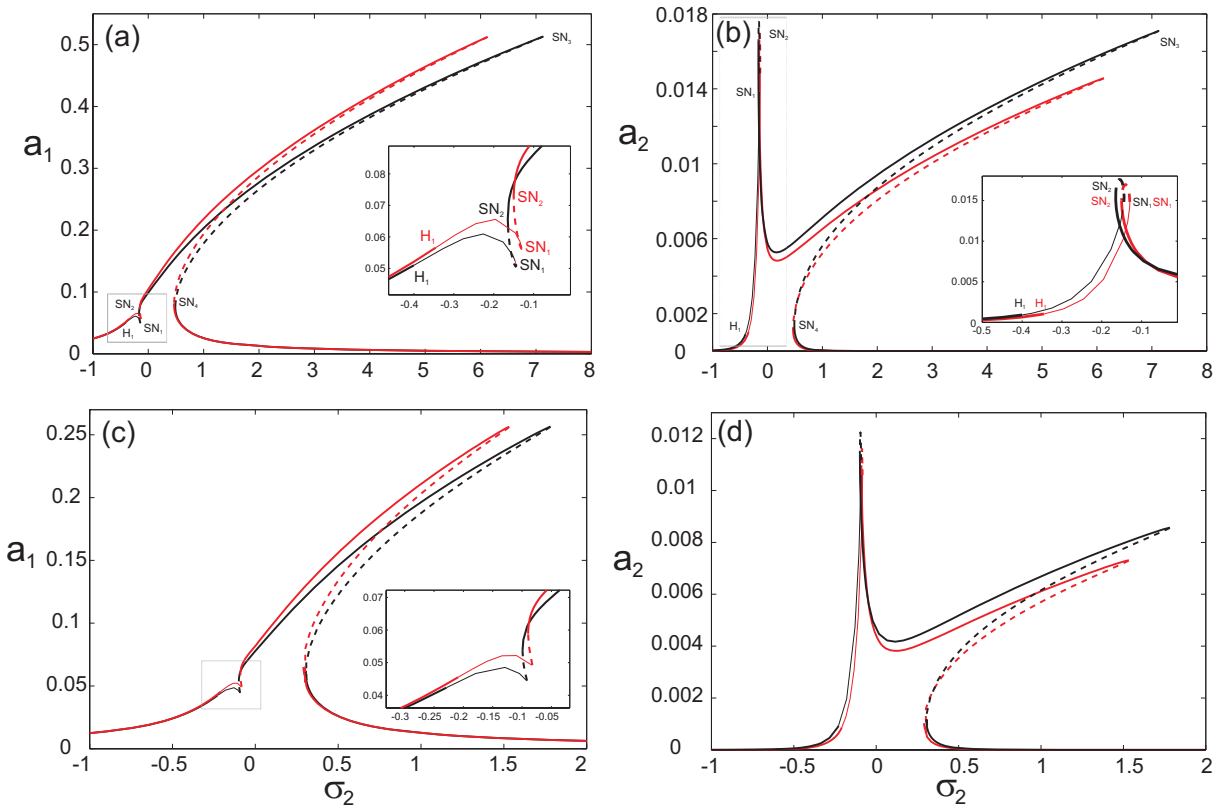

Figure 3. Frequency-response curves for first and second modes, when σ_1 = 0.04, Ω = 326.82 rpm and d_i = 0.05. Considering the forcing amplitude (a-b) f = 0.05 and (c-d) f = 0.025. Solid (dotted) lines denote stable (unstable) equilibrium solutions and thin solid lines denote unstable foci. Black (red) curves correspond to a shear (unsheareable) model.

The response curves exhibit an interesting behavior due to saddle-node bifurcations (where one of the corresponding eigenvalues crosses the imaginary axis along the real axis from the left- to the right-half plane) and Hopf bifurcations (where one pair of complex conjugate eigenvalues crosses the imaginary axis transversely from the left to the right-half plane). As

σ_2 increases from a small value, the solution increases in amplitude and loses stability via a Hopf bifurcation at H_1 and regains its stability via a saddle-node bifurcation at SN_2. The jump effect takes place beyond the saddle-node bifurcations SN_3. An exchange-energy between both modes is observed in the region of the unstable foci solution where the amplitude of the first mode decreases while the second mode amplitude increases considerably.
The effect of the forcing amplitude is clearly proportional in the first mode, where the maximum amplitude decreases to its half value when f decreases to 0.025. However, in the second mode the larger amplitude corresponds to the first peak when f decreases to 0.025. It is due that the second mode does not depend directly on the forcing force but of the internal resonance effect (interaction modes).
The amplitude response obtained disregarding the shear effect is shown in red color curves. It can be observed that the dynamic behavior is similar to that obtained with the present model. In the first mode (Fig. 3a and c), the response reaches the same maximum amplitude value but predicts an earlier jump effect in comparison with the black curve. Contrary, in the second mode the red curves do not reach to the maximum amplitude obtained when the shear effect is considered (black curve). In this case the unstable region predicted for the unshearable model is smaller in comparison with the present model. It is due because to, in spite of the beam slenderness, the second frequency presents a difference of about 32% between both models.

In the second example the beam length is reduced to L = 10m, so the natural frequencies increased as also the rotating speed for the internal resonance condition. The corresponding nonlinear interaction coefficients are presented in Table 2. The coefficients correspond to a specific value of the rotating speed Ω = 861.9 rpm for which ω_1 = 18.95 Hz and ω_2 = 52.85 Hz in the case of the present model and ω_1 = 20.3 Hz and ω_2 = 94.1 Hz when the shear effect in neglected.

Table 2. Coefficients of the modulation equations, Eqs. (30 and 31) for L= 10 m and Ω = 861.9 rpm.

Model	γ_{11}	γ_{12}	γ_{21}	γ_{22}	δ_1	δ_2
With shear	30.9	910.5	-112.1	-669.5	-146.7	6.4
Without shear	26.5	842.3	-87.5	-599.2	-136.5	4.5

The frequency-response curves presented in Figures 4 are similar to the previous case (see Figures 3 c and d). However, in this case the bending of the amplitude curves is larger in comparison with the longer beam (hardening-spring type). It is well known that the effect of shear deformation in more noticeable when the beam length decreases. In this case the beam slenderness is h/L = 0.03 and the difference between both models in the second frequency ω_2 is about 78%.
The jump effect for large values of the detuning parameter σ_1 is characterized by the great amplitude reached previously to the saddle-node bifurcation SN_3. It can be observed from the figures that this amplitude is smaller when the shear effect is neglected. The difference is about the 17% in the SN_3 values obtained by means of both models. In the previous example this discrepancy has been of about the 14%.

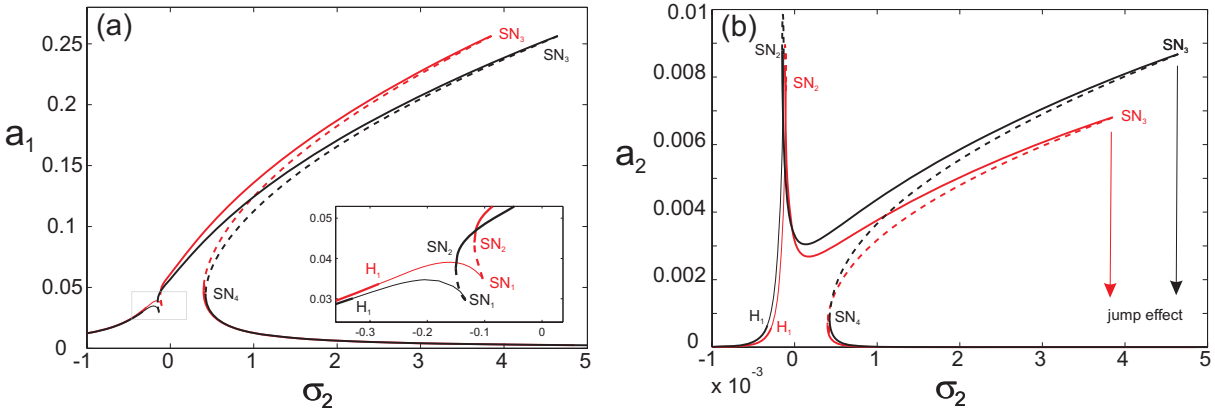

Figure 4. Frequency-response curves for first and second modes, when $f = 0.025$, $\sigma_1 = 0.04$, $\Omega = 861.9$ rpm and $d_i = 0.05$. Solid (dotted) lines denote stable (unstable) equilibrium solutions and thin solid lines denote unstable foci. Black (red) considering (disregarding) shear effect.

In this last example the beam length is reduced to $L = 5$m and the corresponding nonlinear interaction coefficients are presented in Table 3. The coefficients correspond to a specific value of the rotating speed $\Omega = 1040$ rpm for which $\omega_1 = 41.8$ Hz and $\omega_2 = 125.3$ Hz in the case of the present model and $\omega_1 = 61.1$ Hz and $\omega_2 = 369$ Hz when the shear effect in neglected.

Table 3. Coefficients of the modulation equations, Eqs. (30 and 31) for L= 5 m and Ω = 1040 rpm.

Model	γ_{11}	γ_{12}	γ_{21}	γ_{22}	δ_1	δ_2
With shear	433.9	10794.6	-1929.6	-12285.0	-2096.0	99.7
Without shear	325.8	10923.1	-801.1	-5775.5	-1822.5	39.1

The frequency-response curves presented in Figures 5 are computed with a damping modal value of $d_i = 0.1$. The effect of shear deformation is larger in comparison with the previous examples. The slenderness ratio is $h/L = 0.06$ and there is a difference between both models of about 46% for the first frequency ω_2 and 200% in the second frequency ω_2. Following the same comparison as in the previous examples, in this case the saddle-node bifurcation SN_3 computed disregarding the shear effect is located a 23% lower value than the obtained with the present model.

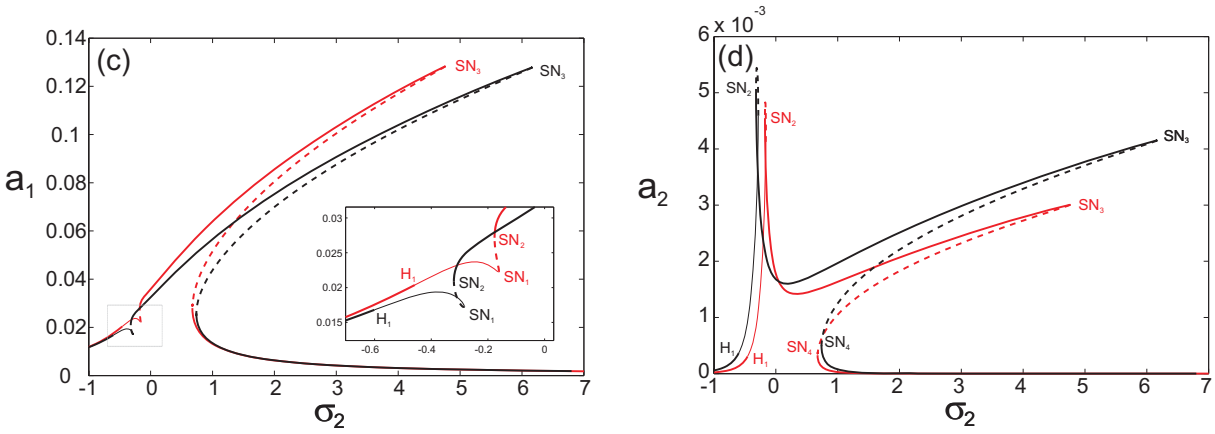

Figure 5. Frequency-response curves for first and second modes, when $f = 0.025$, $\sigma_1 = 0.04$, $\Omega = 1040$ rpm and $d_i = 0.1$. Solid (dotted) lines denote stable (unstable) equilibrium solutions and thin solid lines denote unstable foci. Black (red) considering (disregarding) shear effect.

The influence of the internal detuning parameter σ_1 is analyzed in Figure 6, where the effect

of shear deformation is also illustrated. The frequency-response curves are computed with the same damping modal value of the previous example, but the internal detuning parameter is far away from the perfect resonance condition $\sigma_1 = 4$. It can be observed that the curves are similar to the previous Figures, however, for large values of σ_2 appear another unstable foci solution bounded for two Hopf bifurcation at $\sigma_2 = 0.89$ (H_2) and $\sigma_2 = 1.087$ (H_3). The size of this new unstable solution is smaller for the case of disregard the shear effect (red curve). This last behavior can be easily observed in the right little frame showed in the Figure 6a. The response of the second mode seems to be similar to the previous examples, but the multiplicity of the solutions between $0 > \sigma_2 > 1$ becomes its dynamic behavior more complicated, depending mainly of the initial conditions. Finally, the amplitude peak of the second mode is noticeably larger when $\sigma_1 = 4$ in comparison with the previous case (see Figure 5b), while the bifurcation value SN_3 is exactly identical in both examples.

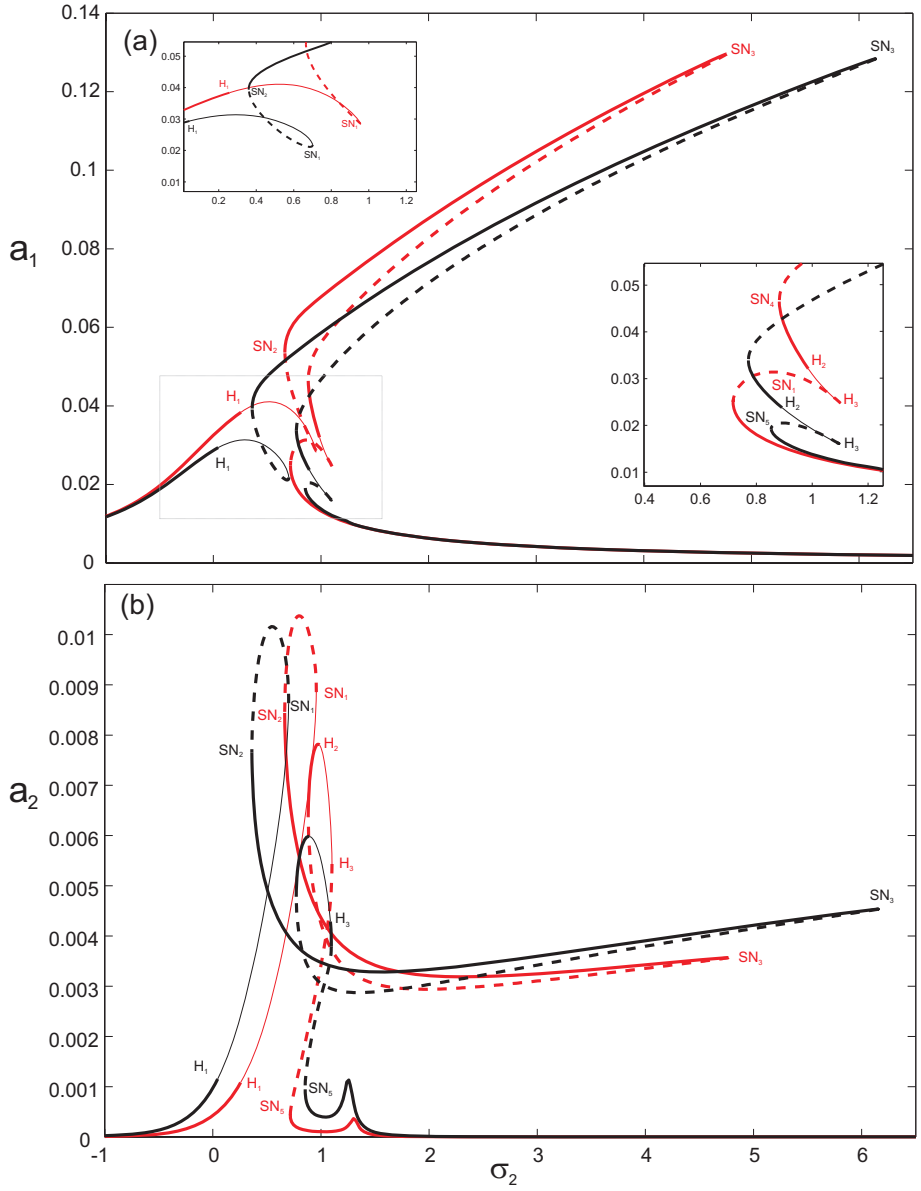

Figure 6. Frequency-response curves for (a) first and (b) second modes, when $f = 0.025$, $\sigma_1 = 4$, $\Omega = 1040$ rpm and $d_i = 0.1$. Solid (dotted) lines denote stable (unstable) equilibrium solutions and thin solid lines denote unstable foci. Black (red) considering (disregarding) shear effect.

6 CONCLUSIONS

The nonlinear planar response of a cantilever rotating box beam to a principal parametric resonance of its first flexural mode is investigated. The beam is subjected to a harmonic transverse load in the presence of internal resonance. The internal resonance can be activated for a range of the beam rotating speed, where the second natural frequency is approximately three times the first natural frequency. Geometric cubic nonlinear terms are included in the equation of motion due to midline stretching of the beam. The material is considered to be linear elastic and the cross-section properties are assumed to be constant given the assumption of small strains.

Nonlinear normal modes are computed by applying the method of multiple scales directly to the governing integral-partial-differential equation and associated boundary conditions. Two sets of four first-order nonlinear ordinary-differential equations describing the modulation of the amplitudes and phases of the first two modes are derived.

The resonant behavior is illustrated by frequency-response curves for a sequence of lamination of {*0/0/0/0*}. The influence of the shear deformation effect is shown in the curves considering different rotation speed, damping, detuning parameters, force amplitudes and beam lengths.

Numerical results show that the frequency-response curves exhibit a hardening type behavior. The analysis presented demonstrates that the equilibrium solutions are influenced by the transverse shear effect. When this effect is ignored the amplitude of vibration is reduced significantly, thus altering the dynamic response of the beam. This alteration can lead to an incorrect stability prediction of the periodic solutions. For example, the unstable region characterized by the jump effect is smaller when the shear effect is neglected. Therefore the Euler-Bernoulli model predicts a less critical dynamic scenario than the present shear model.

On the other hand, when the internal detuning parameter is varied from its perfect condition, the frequency-response curves exhibit a more complex behavior.

ACKNOWLEDGEMENTS

The present study was sponsored by Secretaría de Ciencia y Tecnología, Universidad Tecnológica Nacional, and by CONICET.

REFERENCES

Apiwattanalunggarn P., Shaw S.W., Pierre C., and Jiang D. Finite-Element-Based Nonlinear Modal Reduction of a Rotating Beam with Large-Amplitude Motion. *Journal of Vibration and Control*, 9:235-263, 2003.

Barbero E.J., *Introduction to Composite Material Design*. Taylor and Francis Inc, 1999.

Hodges D.H. and Rutkowski, M.J. Free-vibration analysis of rotating beams by a variable-order finite-element method. *AIAA Journal*, 19:1459-1466, 1981.

Leissa A. Vibrational aspects of rotating turbomachinery blades. *ASME Applied Mechanics Reviews*, 34:629-635, 1981.

Librescu L. *Thin –Walled Composite Beams*¸ Springer, Dordrecht, 2006.

Machado S.P. and Cortínez V.H. Lateral buckling of thin-walled composite bisymmetric beams with prebuckling and shear deformation. *Engineering Structures*, 27:1185-96, 2005a.

Machado S.P. and Cortínez V.H. Non-Linear model for stability of thin walled composite beams with shear deformation. *Thin wall Structures*, 43:1615-45, 2005b.

Machado, S.P., Filipich, C.P., and Cortínez, V.H. Parametric vibration of thin-walled

composite beams with shear deformation. *Journal of Sound and Vibration*, 305:563–581, 2007.
Machado S.P. and Cortínez V.H. Dynamic stability of thin-walled composite beams under periodic transverse excitation. *Journal of Sound and Vibration*, 321:220-41, 2009.
Machado S.P. Interaction of combined loads on the lateral stability of thin-walled composite beams. *Engineering Structures*, 32:3516-27, 2010.
Machado S.P. and Saravia M.C. Non-linear dynamic response of a rotating thin walled composite beam. *Mecánica Computacional*, Vol. XXIX:1203-1224, 2010.
Nayfeh A.H., Nayfeh J.F., and Mook D.T. On methods for continuous systems with quadratic and cubic nonlinearities. *Nonlinear Dynamics* 3:145–162, 1992.
Nayfeh A.H. and Mook, D.T. *Nonlinear Oscillations*, Wiley, 1979.
Nayfeh A.H. and Balachandran B. Modal interactions in dynamical and structural systems, *Applied Mechanics Reviews*, 42:175-201, 1989.
Nayfeh A.H. and Balachandran B. *Applied Nonlinear Dynamics: analytical computational and Experimental Methods*, Wiley-Interscience, 1995.
Nayfeh A.H. *Nonlinear Interactions*, Wiley, 1996.
Pesheck E., Pierre C., and Shaw S.W. Accurate reduced order models for a simple rotor blade model using nonlinear normal modes. *Mathematical and Computer Modeling*, 33:1085–1097, 2001.
Pesheck E., Pierre C., and Shaw S.W., Modal reduction of a nonlinear rotating beam through nonlinear normal modes. *ASME Journal of Vibration and Acoustics*, 124:229–236, 2002a.
Pesheck E., Pierre C., and Shaw S.W. A new Galerkin-based approach for accurate nonlinear normal modes through invariant manifolds. *Journal of Sound and Vibration*, 249:971–993, 2002b.
Sapkás A. and Kollár L.P. Lateral-torsional buckling of composite beams. *International Journal of Solids and Structures*, 39:2939-63, 2002.
Sapountzakis E.J. and Mokos V.G. Shear deformation effect in nonlinear analysis of spatial beams. *Engineering Structures*, 30:653-63, 2008
Schilhansl M.J. Bending frequency of a rotating cantilever beam. *ASME Journal of Applied Mechanics*, 25:28-30, 1958.
Shaw S.W. and Pierre C. Normal modes for non-linear vibratory systems. *Journal of Sound and Vibration*, 164:85–124, 1993.
Shaw S.W. and Pierre C. Normal modes of vibration for non-linear continuous systems. *Journal of Sound and Vibration*, 169:319–347, 1994.
Shaw S.W., Pierre C., and Pesheck E. Modal analysis-based reduced-order models for nonlinear structures-an invariant manifold approach. *The Shock and Vibration Digest*, 31:3–16, 1999.
Turhan O. and Bulut G. On nonlinear vibrations of a rotating beam. *Journal of Sound and Vibration*, 322:314–335, 2009.
Wang J.T.S., Mahrenholtz O., and Bohm J. Extended Galerkin's method for rotating beam vibrations using Legendre polynomials. *Solid Mechanics Archives*, 1:341-365, 1976.

APPENDIX

The terms used in the Eqs. (29), (30) and (31) are defined as:

$$\Gamma_1 = -2i\omega_1\vartheta_1\left(A_1' + \mu A_1\right) + \left(3\vartheta_1'' \int_0^1 \vartheta_1'^2 dx\right) A_1^2\bar{A}_1 + \left(2\vartheta_1'' \int_0^1 \vartheta_1'\vartheta_2' dx + \vartheta_2'' \int_0^1 \vartheta_1'^2 dx\right) A_2\bar{A}_1^2 e^{i\sigma_1 T_1} + \left(4\vartheta_2'' \int_0^1 \vartheta_1'\vartheta_2' dx + 2\vartheta_1'' \int_0^1 \vartheta_2'^2 dx\right) A_1 A_2 \bar{A}_2, \tag{44}$$

$$\Gamma_2 = -2i\omega_2\vartheta_2\left(A_2' + \mu A_2\right) + \left(3\vartheta_2'' \int_0^1 \vartheta_2'^2 dx\right) A_2^2\bar{A}_2 + \left(\vartheta_1'' \int_0^1 \vartheta_1'^2 dx\right) A_1^3 e^{-i\sigma_1 T_1} + \left(4\vartheta_1'' \int_0^1 \vartheta_1'\vartheta_2' dx + 2\vartheta_2'' \int_0^1 \vartheta_1'^2 dx\right) A_1 A_2 \bar{A}_1, \tag{45}$$

$$\mu_m = \int_0^1 \mu\vartheta_m^2 dx \tag{46}$$

$$\gamma_{mm} = \frac{3}{8\omega_m}\Gamma_{mmmm} \tag{47}$$

$$\gamma_{mn} = \frac{1}{8\omega_m}\left(4\Gamma_{mmnn} + 2\Gamma_{mmnn}\right), \quad m \neq n \tag{48}$$

$$\delta_1 = \frac{1}{8\omega_1}\left(2\Gamma_{1112} + \Gamma_{1211}\right), \tag{49}$$

$$\delta_2 = \frac{\Gamma_{2111}}{8\omega_2}, \tag{50}$$

$$\Gamma_{mnpq} = -\left(\int_0^1 \vartheta_m\vartheta_n'' dx\right)\left(\int_0^1 \vartheta_p'\vartheta_q' dx\right), \tag{51}$$

$$f_m = \frac{1}{\omega_m}\int_0^1 f\vartheta_m dx \tag{52}$$